Fourth-order coherent Raman spectroscopy in a time domain: applications to buried interfaces

Nomoto, Tomonori

Onishi, Hiroshi

Fourth-order coherent Raman spectroscopy in a time domain: applications to buried interfaces

Tomonori Nomoto,[a, b] and Hiroshi Onishi*[a, b]

Receipt/Acceptance Data **[DO NOT ALTER/DELETE THIS TEXT]**
Publication data **[DO NOT ALTER/DELETE THIS TEXT]**
DOI: 10.1039/b000000x [DO NOT ALTER/DELETE THIS TEXT]

A Raman-based, nonlinear optical spectroscopy is a promising method of observing vibrational modes localized at buried interfaces. The principles of the Raman excitation and interface-selective detection of coherent vibrations are described. Applications to air-liquid, liquid-liquid, air-solid, liquid-solid, and solid-solid interfaces are reviewed.

1. Introduction

There is an increasing need to apply chemistry to buried interfaces. Natural as well as artificial conversion of energy and materials mostly occurs at interfaces between two different media. When an interface of interest is exposed to a vacuum, electron-based or ion-based methods are available to determine the chemical composition and molecular structure of the top most atom layers. The limited penetration depth of the charged particles results in vertical resolution of analysis. When the interface is not in a vacuum, which is often the case with interfaces relevant to chemistry and biochemistry, analyses of the interface surrounded by some medium is necessary. This is not easy at all. Charged particles with limited penetration depth do not appear on the interface to be analyzed.

Vibrational sum-frequency (VSF) spectroscopy,[1] a photon-based method, meets two requirements for analyses of buried interfaces; the vertical resolution of analysis and penetration ability of the probe. Sum-frequency light is generated at an interface irradiated with infrared (IR) and visible lights. The probability of generation is governed by a second-order susceptibility $\chi^{(2)}$ to be zero in any media with inversion symmetry. A finite probability is allowed at interfaces where the symmetry breaks. The probability, when allowed, is enhanced by the vibrational resonance of the IR light. The SF light intensity as a function of the IR wavenumber provides a vibrational spectrum at the interface.

VSF spectroscopy is successful in probing interfaces exposed to vapor.[2-5] Infrared light is, however, absorbed by liquids or solids. Access to interfaces buried in condensed media has been achieved by irradiating probe light from the side of a weak IR-absorptive material.[6-9]

The authors propose application of an IR-free, Raman-based nonlinear optical method to buried interfaces, which was originally developed in 1997 by Chang, Xu and Tom to observe coherent phonons at GaAs surfaces.[10] Vibrations are pumped with near-infrared or visible light via a stimulated Raman transition instead of IR resonant transition used in the VSF scheme. Another ability of this Raman-based method is to access low-frequency vibrations. It is difficult to prepare low-frequency IR light compatible with VSF generation. A specifically modified tabletop laser light source[11] or a free-electron laser facility[12] is required to observe a VSF spectrum of wavenumbers below 1000 cm^{-1}. Low-frequency vibrations are important in dissipating excess energy released in endothermic reactions at interfaces. Lateral and vertical transport of molecules across an interface is initiated by multiple excitation of low-frequency modes including frustrated rotations and frustrated translations.

The principle and experimental scheme of the Raman-based method is reviewed in sections 2 and 3. Applications to air-liquid, liquid-liquid, air-solid, liquid-solid, and solid-solid interfaces are described in sections 4-8 including the latest technical developments in section 9. Readers find a comprehensive review[13] of coherent vibrations at solid surfaces observed in the ultrahigh vacuum. This Invited Article is focused on coherent vibrations at buried interfaces.

2. Coherent excitation and interface-selective detection of Raman-active modes

A light pulse of a center frequency Ω impinges on an interface. A Raman-active mode of nuclear motion is coherently excited via impulsive stimulated Raman scattering, when the time width of the pulse is shorter than the period of the vibration. The frequency width of this ultrashort light pulse exceeds the energy gap between the ground state *g* and a vibrational excited state *v*. The frequency width of the pulse is related to the Fourier transformation of the time width, according to the energy-time uncertainty relation. When the full width at half maximum (fwhm) of a Gaussian pulse is 20 fs, its bandwidth is 740 cm^{-1} as the fwhm. Frequency components Ω_L and Ω_S are present in the pulse and are used to generate the vibrational coherence, where Ω_L-Ω_S is equal to the vibrational frequency ω.

Another light pulse of frequency Ω comes at a time delay t_d and interacts with the vibrationally excited molecules. The intensity of the Ω light transmitted through the interface or reflected at the interface is modulated as a function of the delay. The modulation is Fourier-transformed to provide the frequency and phase of the coherent vibration. The decay of

[a] *Department of Chemistry, Kobe University, Rokko-dai, Nada, Kobe, 657-8501 Japan.*
[b] *Core Research for Evolutional Science and Technology, Japan Science and Technology Agency, Honmachi, Kawaguchi, 332-0012 Japan.*
E-mail: oni@kobe-u.ac.jp

the coherence is traced with the modulation amplitude. This series of optical transitions shown in Fig. 1(a) contains three incident electric fields (Ω_L, Ω_S, Ω) and offers bulk-sensitive, time-domain detection of vibrational coherence. The whole portion of the molecules having interacted with the pump pulse contributes to the generation of the optical response. This method has been successfully applied to bulk liquids,[14] bulk solids,[15, 16] and molecular submonolayers,[17, 18] and is known as third-order Raman spectroscopy in the time domain.

To offer interface-selective detection of the Raman-pumped vibrational coherence, one more incident electric field is required. A fourth-order optical response is thereby generated. The requirement is fulfilled by observing the second harmonic (SH) light generated at the interface instead of the transmitted Ω light. The second-harmonic probe scheme contains four incident electric fields (Ω_L, Ω_S, Ω, Ω) as shown in Fig. 1(b), and the signal field E_{fourth} is proportional to the fourth-order response function. The even order of the optical transition ensures the interface-selective observation of vibrational coherence. The two-photon transition probing the coherence is equivalent to a hyper-Raman scattering from v to g.[19] The cross section of the whole pump-and-probe transitions is therefore proportional to the product of the Raman tensor for the pump and the hyper-Raman tensor for the probe.

Insert Fig. 1.

Fig. 1 Impulsive stimulated Raman excitation of a molecular vibration. Ω_L and Ω_S are high-frequency and low-frequency components of the pump light pulse. A probe pulse of frequency Ω interacts with the vibrational coherence to present the optical response of (a) the fundamental frequency $\Omega+\omega\approx\Omega$ and (b) the second harmonic frequency $2\Omega+\omega\approx2\Omega$.

When two or more modes of vibration are excited, the fourth-order Raman field E_{fourth} is presented as the sum of exponentially decayed modulations,

$$E_{\mathrm{fourth}}(t_{\mathrm{d}},\ 2\Omega) \propto \sum_{\mathrm{v}} A_{\mathrm{v}} \cos(\omega_{\mathrm{v}} t_{\mathrm{d}} + \varphi_{\mathrm{v}}) \exp(-t_{\mathrm{d}}/T_{\mathrm{v}}), \quad (1)$$

where A_v, ω_v, φ_v, and T_v are the amplitude, frequency, phase, and dephasing time of each mode. This presentation is analogous to what has been established in third-order Raman spectroscopy.[20] The time-domain response is Fourier-transformed to a frequency spectrum of the fourth-order susceptibility, $\chi^{(4)}(\omega_v)$.

The efficiency of the impulsive stimulated Raman excitation is enhanced when an electronic transition from g to an electronic state e is resonant with the photon energy. When the transition from g to e is resonant with the energy of one photon, a cosine-like oscillation is generated with φ_v=0 or π. If the photon energy is out of the electronic resonance, a sine-like oscillation is expected with φ_v=π/2 or 3π/2.

In addition to the fourth-order field E_{fourth}, the probe light generates two SH fields; the pump-free SH field $E_0(2\Omega)$, and the pump-induced non-modulated SH field. The ground-state population is depleted by the pump irradiation. The latter term $E_{\mathrm{non}}(t_{\mathrm{d}}, 2\Omega)$ is a virtual electric field to represent the decrease of the SH field. Time-resolved second harmonic generation (TRSHG) has been applied to observe $E_{\mathrm{non}}(t_{\mathrm{d}}, 2\Omega)$ with a picosecond time resolution.[21-26] The fourth-order field interferes with the two SH fields to be detected in a heterodyned form.

The pump-affected intensity of SH light $I(t_{\mathrm{d}}, 2\Omega)$ is given by,

$$\frac{I(t_{\mathrm{d}},\ 2\Omega)}{I_0(2\Omega)} = \frac{\left|E_0(2\Omega) + E_{non}(t_{\mathrm{d}},\ 2\Omega)e^{i\Phi} + E_{fourth}(t_{\mathrm{d}},\ 2\Omega)e^{i\phi}\right|^2}{\left|E_0(2\Omega)\right|^2} \quad (2)$$

with respect to the pump-free intensity $I_0(2\Omega)$. Φ is the phase shift of $E_{\mathrm{non}}(t_{\mathrm{d}}, 2\Omega)$ relative to $E_0(2\Omega)$ and assumed to be zero, because E_{non} and E_0 are generated in a common, second-order transition. ϕ represents the phase shift of E_{fourth} relative to $E_0(2\Omega)$. With E_{fourth} being much smaller than the other terms, equation (2) is simplified as,

$$E_{\mathrm{fourth}}(t_{\mathrm{d}}, 2\Omega)\, E_{\mathrm{second}}(t_{\mathrm{d}}, 2\Omega) \propto I(t_{\mathrm{d}}, 2\Omega) - I_{\mathrm{second}}(t_{\mathrm{d}}, 2\Omega) \quad (3)$$

where $E_{\mathrm{second}}(t_{\mathrm{d}}, 2\Omega) = E_0(2\Omega) + E_{\mathrm{non}}(t_{\mathrm{d}}, 2\Omega)$. $I_{\mathrm{second}}(t_{\mathrm{d}}, 2\Omega)$ is the SH light intensity relevant to E_{second} and determined with a nonoscillatory numerical function fitted to the observed $I(t_{\mathrm{d}}, 2\Omega)$. The right-hand side of equation (3) thus represents the intensity modulation of the SH light, $I_{\mathrm{fourth}}(t_{\mathrm{d}}, 2\Omega)$. On the left-hand side, the fourth-order field E_{fourth} is multiplied with E_{second}.

The fourth-order field is heterodyned with the second-order field. The intensity modulation of the signal light, the observable, is proportional to the amplitude of E_{fourth} and hence to the number of coherently vibrating molecules. The heterodyne detection of an electric field is advantageous over the homodyne detection, when the field of interest is weak. This is particularly the case for our fourth-order response. The advantage of the heterodyne detection, when available on interfaces, has been demonstrated in SH[27, 28] and VSF[29] studies.

Hirose et al.[30] proposed a homodyne scheme to achieve the backgroud-free detection of E_{fourth}. With pump irradiation in a transient grating configuration, the fourth-order field propagates in a direction different from that of the scond-order field because of different phase match conditions. The fourth-order fields is homodyned to make $I_{\mathrm{fourth}}(t_{\mathrm{d}}, 2\Omega)$ and spatially filtered from the second-order response $I_{\mathrm{second}}(t_{\mathrm{d}}, 2\Omega)$.

3. Experimental methods

Figure 2 illustrates the spectrometer in our laboratory. A noncollinear optical parametric amplifier (TOPAS-white, Quantronix) is pumped by a Ti:sapphire regenerative amplifier (Hurricane, Spectra Physics, 800 nm, 90 fs, 1 kHz). The time width of the parametrically amplified light pulse is less than 20 fs, and the wavelength is tunable at 500-750 nm. A p-polarized pump and p-polarized probe pulses are focused at an interface with an incident angle θ of 50°. The spot diameter of the focused beams is 0.1 mm. The p-polarized SH light beam emitted to the reflected direction is conducted to a photomultiplier tube. The multiplier output is gated with a boxcar integrator and sent to a PC on a pulse-to-pulse basis.

The pump pulse is chopped at 500 Hz. The pump-on signal and pump-off signal are separately accumulated, and the former is divided by the latter. The time origin is determined by monitoring the SH light intensity emitted from the interface. A more detailed description is available.[31]

Insert Fig. 2.

Fig. 2 A fourth-order coherent Raman spectrometer with a liquid-liquid interface. NOPA: noncolinear optical parametric amplifier, BS: beam splitter, VND: variable neutral density filter, PD: photodiode, P: Glan-Taylor prism, PMT: photomultiplier tube.

When a liquid (and probably solid) layer of 0.1 mm or thicker covers the interface, the impinging light pulses experience group velocity dispersion before arriving at the interface. This undesired dispersion should be compensated by adding an extra negative chirp in the noncollinear amplifier.

The time resolution of the instrument determines the wavenumber-dependent sensitivity of the Fourier-transformed, frequency-domain spectrum. A typical instrumental response of the spectrometer of Fig. 2 is 23 fs. With this time-domain response, a Gaussian function having a half width at half maximum (hwhm) of 640 cm^{-1} centered at 0 cm^{-1} represents the wavenumber-dependent sensitivity. Frequency spectra in this article are presented without correcting the sensitivity.

4. Air-liquid interface

Fujiyoshi et al. first observed the fourth-order coherent Raman spectrum of a liquid surface.[32] The same authors later reported a spectrum with an improved signal-to-noise ratio and different angle of incidence.[31] An organic dye solution, oxazine 170 solved in water, was placed in air and irradiated with pump and probe pulses. The pump and probe wavelength was tuned at 630 nm to be resonant with the one-photon electronic transition of the dye. The probability of the Raman transition to generate the vibrational coherence was enhanced as well as the hyper-Raman transition to generate the SH field.

When the photon energy was resonant with the electronic transition, the ground-state population was depleted by the pump irradiation and restored with the time delay. The raw intensity of SH light was accordingly damped at t_d=0 and recovered within picoseconds as seen in panel (b) of Fig. 3. Intensity modulation due to coherent vibrations was superimposed on the non-modulated evolution. The coherent vibrations continued for picoseconds on this solution surface. The non-modulated component was fitted with a multiexponential function and subtracted. Panel (c) shows the modulated component $I_{\mathrm{fourth}}(t_d, 2\Omega)$, which is proportional to the fourth-order field multiplied with E_{second} according to equation (3).

The modulation was converted to a frequency-domain spectrum via Fourier transformation. The window function multiplied to the raw modulation determined the wavenumber resolution of the transformed spectrum. Our typical number was 6 cm^{-1} as the fwhm. Panel (d) presents the transformed spectrum. Negative, symmetric-shape bands are present at 535, 561, 594, 618, and 683 cm^{-1} in the real part, together with dispersive-shape bands in the imaginary part at the corresponding wavenumbers. This feature indicates the phase of fourth-order field ϕ to be π. Cosine-like coherence was generated in the five vibrational modes, being consistent to the phase of vibration expected by an impulsive stimulated Raman transition resonant with an electronic excitation.

The wavenumber of the observed bands are identical with those of the spontaneous Raman spectrum of the solution and oxazine solid.[31] The impulsive stimulated Raman transition can initiate coherent vibrations also in the electronic excited state. By interacting with the probe light pulses the coherence in the excited state, if any, provides modulated SH light. However, there was no sign of the excited-state vibrations superimposed on the ground-state bands in the spectrum of Fig. 3.

The surface of a coumarin 314 solution was examined with pump irradiation in a transient grating configuration.[30] A nonoscillatory response was observed with a pump wavelength of 800 nm nonresonant to the electronic transitions of coumarin.

Insert Fig. 3.

Fig. 3 Fourth-order coherent Raman spectroscopy at an air-liquid interface. The orientation of oxazine 170 at an air-solution interface is illustrated in (a) after Steinhurst and Owrutsky.[26] (b) The raw SH intensity, (c) the modulated component, and (d) Fourier-transformed spectrum are presented. The solution surface was irradiated with *p*-polarized pump (5 mJ cm^{-2}) and *p*-polarized probe (2.5 mJ cm^{-2}) pulses of a 630-nm wavelength.

5. Liquid-liquid interface

A 0.2-mm thick hexadecane layer was placed on the oxazine solution.[31] Figure 4 shows the SH light intensity, modulated component, and Fourier-transformed spectrum. The spectrum on the hexadecane-solution interface reproduced the spectrum on the air-solution interface. The center wavenumber and relative strength of the five bands are insensitive to the hexadecane overlayer.

Here we ask the question why the vibrations of oxazine are insensitive to the composition of the interface. Vibrations in a chromophore is thought to be sensitive to the solvent structure around the chromophore.[6, 8, 23] This was not the case for this particular chromophore.

The spontaneous Raman spectrum of oxazine was observed in the bulk solution and bulk solid. Dye monomers are equilibrated with dimerized species in the solution.[26] The solvated monomer, solvated dimer, and solid dye are in different dielectric environments and experience different inter-molecular interactions. The observed Raman bands are nevertheless identical with each other, and reproduce the two spectra shown in Figs. 3 and 4. It is hence not surprising that the oxazine vibrations are insensitive to the interface composition.

Insert Fig. 4.

Fig. 4 Fourth-order coherent Raman spectroscopy at a liquid-liquid interface. A 0.2-mm thick hexadecane layer was placed on the oxazine solution of Fig. 3. (a) The raw intensity of SH light, (b) modulated component, and (c) Fourier-transformed spectrum. The interface was irradiated with *p*-polarized pump (5 mJ cm^{-2}) and *p*-polarized probe (2.5 mJ cm^{-2}) beams of a 630-nm wavelength.

6. Air-solid interface

A number of solid compounds have been examined to date with fourth-order coherent Raman spectroscopy. Chang et al. invented this technique by observing coherent phonons in GaAs.[10] Cesium-deposited[33-35] and potassium-deposited[36] surfaces of platinum were extensively studied. Manipulation of coherent phonons were further demonstrated on Cs/Pt by using pump pulse trains.[37] Magnetic properties have been studied on Gd films.[38, 39] Most of these studies were performed in the ultrahigh vacuum.

In sections 6 and 7 coherent phonons of a TiO_2 surface placed in air and liquid are described. TiO_2 is a wide-bandgap, prototypical metal oxide. The (110) plane of rutile TiO_2 is the most extensively studied single-crystalline surface of metal oxide.[40] Atomically flat surfaces are routinely prepared in a vacuum and characterized with various techniques including probe microscopes.[41] The vacuum-prepared surface may be contaminated when taken out of the vacuum chamber and exposed to laboratory air. White et al.[42] found that a chemisorbed trimetylacetate (TMA) monolayer, which is shown in panel (a) of Fig. 5, passivates the surface against chemisorption of water.

The coherent vibration on the TMA-covered surface was observed in air with pump and probe pulses of a 630-nm wavelength.[43] This red light is not resonant with the bandgap excitation of TiO_2 (3 eV). The coherent response presented in panels (b) and (c) decays much more rapidly than the modulation on the solution surfaces described in the preceding sections. The energy localized in the vibrational modes efficiently dissipates in the infinite -Ti-O- network of the solid.

Four major bands are recognized at 180, 357, 444, and 826 cm^{-1} in the Fourier-transferred spectrum of panel (d). The first band appears at the position of an IR-active, bulk phonon mode of E_u symmetry.[44] The wavenumbers of the third and fourth bands agree with those of Raman-active bulk phonons, an E_g-symmetry mode and a B_{2g}-symmetry mode.[45] In the bulk rutile having a D_{4h} symmetry, a Raman-active mode is inactive for hyper-Raman transitions.[19] Hence, the fourth-order transition of the three bands at 180, 444, and 826 cm^{-1} is forbidden in the bulk rutile. The wavenumbers of surface phonons are close to those of bulk phonons, indicating that the bulk modes are only slightly modified by the presence of the surface boundary condition. On the other hand, bulk phonon modes are absent in wave numbers near 357 cm^{-1}, the center-frequency of the second band. According to electron energy loss studies done in the vacuum,[46, 47] the TMA-free TiO_2(110) exhibits surface optical phonons (Fuchs-Kliewer modes) at 772-756, 434-418, and 370-353 cm^{-1} consistent with the fourth-order Raman results presented here.

The most intense 826-cm^{-1} band is broader than the other three bands. The broadened band can best be understood with an eigen frequency distribution in the observed portion of the surface. Indeed, the symmetric peak in the imaginary part of the Fourier-transformed spectrum is fitted with a Gaussian function rather than with a Lorenz function. The bandwidth was estimated to be 56 cm^{-1} by considering the instrumental resolution (15 cm^{-1} in this particular spectrum). This number is much larger than that of the bulk B_{2g} mode (25 cm^{-1}).[45] Further studies are needed to interpret the different bandwidths.

The shape of three bands at 180, 444 and 826 cm^{-1} is negative and symmetric in the imaginary part of the Fourier-transformed spectrum, while dispersive in the real part. The phase of the fourth-order field ϕ is thus $3\pi/2$ suggesting sine-like oscillation of atoms. The phase shift from a cosine function to a sine function is evidence for the impulsive stimulated Raman excitation nonresonant with the electronic transition of TiO_2.

Insert Fig. 5.

Fig. 5 Fourth-order coherent Raman spectroscopy at an air-solid interface. (a) The structure of the TMA-covered TiO_2(110) surface. (b) The raw intensity of SH light, (c) modulated component, and (d) Fourier-transformed spectrum observed on the TMA-covered surface placed in air. The surface was irradiated with *p*-polarized pump (14 mJ cm^{-2}) and *p*-polarized probe (6 mJ cm^{-2}) beams of a 630-nm wavelength.

7. Liquid-solid interface

The authors have just started application to a liquid-solid interface. A TMA-covered TiO_2(110) surface was prepared in the vacuum and immersed in a 0.1 M aqueous solution of HCl. The results are presented in Fig. 6. The thickness of the solution was 0.2 mm. Three phonon bands were apparent at 826, 369 and 178 cm^{-1}. The center frequency and bandwidth reproduced those observed on the air-TiO_2 interface. On the other hand, the band at 444 cm^{-1} was absent on the solution-TiO_2 interface. It remains an open question as to why a phonon band is sensitive to the composition of the interface while the others are not.

Insert Fig. 6.

Fig. 6 Fourth-order coherent Raman spectroscopy at a liquid-solid interface. (a) The raw intensity of SH light, (b) modulated component, and (c) Fourier-transformed spectrum observed on a TiO_2(110) surface prepared in the vacuum and immersed in a HCl solution. The surface was irradiated with *p*-polarized pump (5 mJ cm^{-2}) and *p*-polarized probe (5 mJ cm^{-2}) beams of a 630-nm wavelength.

8. Solid-solid interface

Coherent phonons were created at the metal-semiconductor interface of a GaP photodiode and detected as the modulation of SH light intensity.[48] In stacked GaInP/GaAs/GaInP layers a number of coherent phonon modes were observed at 8-12 THz (270-400 cm^{-1}).[49] A band at 9.4 THz (310 cm^{-1}) was assigned to an optical phonon mode localized at the GaAs/GaInP interface, while others came from bulk modes of the semiconductors. The dephasing time of the coherent phonons were determined on differently prepared samples and related to the growth temperature. Imperfections remained in the layers prepared with a lower temperature to cause dephasing.

9. Extension to frequency-domain detection

One latest technical development is the direct observation of $\chi^{(4)}$ in the frequency domain. In the optical scheme shown in Fig. 1, two femtosecond light pulses are used to pump and probe the coherent vibrations at an interface. Instead, Yamaguchi and Tahara[50] irradiated a solution surface with a white light continuum pulse and a narrow-bandwidth picosecond pulse of frequency Ω simultaneously. Vibrational coherence having different frequencies is generated in a stimulated Raman transition caused by the continuum and the narrow-bandwidth light. The energy distribution of the vibrational excited state *v* is projected on the narrow-bandwidth SH light produced in the hyper-Raman transition from *v* to *g*. Different energy components thereby included in the picosecond SH light are simultaneously detected by using a polychrometer with a multichannel CCD. A frequency-domain spectrum of the coherent vibrations is determined without scanning the pump-probe delay. On the surface of a rhodamine 800 solution, intra-molecular bands at 1200, 1350, 1500, 1650, and 2220 cm^{-1} were observed with this method. The wavenumber resolution was limited by the bandwidth of the picosecond light pulse, 20 cm^{-1} in that work.[50]

In the time-domain detection of the vibrational coherence the intensity oscillation of the optical response is Fourier-transformed to a frequency-domain spectrum. The high-wavenumber limit of the spectral range is determined by the time width of the pump and probe pulses, as described in section 2. Actually, the highest-wavenumber band previously identified in time-domain fourth-order coherent Raman spectrum is the phonon band of TiO_2 at 826 cm^{-1}. [43] The direct observation of frequency-domain spectrum is free from this regulation. On the other hand, the narrow-bandwidth pulse stretched to picoseconds should be less intense than the non-stretched pulse that was used in the time-domain method. The limited intensity of the probe light may cause a problem in detecting weak optical response.

10. Concluding remarks

Successful applications of fourth-order time-domain Raman spectroscopy are presented in this article. Interface-selective detection of Raman-active vibrations is now definitely possible at buried interfaces, while the technique is in a demonstration phase.

We can not ignore drawbacks of this method. Because of the high-order optical transitions, the signal intensity is small. One-photon resonant enhancement of Raman-pump probability was used in most reported works. The observable range of materials is somehow limited as a result, while wavelength-tunable light sources are helpful to expand the range[32]. Although the power of a tabletop laser light source has improved year by year, the damage threshold of target interfaces is severe with intense irradiation. When undesired second-order or third-order optical transitions occur in the condensed phase covering the interface, the fourth-order response is overwhelmed by the undesired responses. Nevertheless, the authors are optimistic about the future of this method. There is much room for technical improvements in the time domain detection and also in the frequency domain detection.

We can recognize the fourth-order coherent Raman spectroscopy to be a Raman spectroscopy with interface selectivity. Coherent vibrations are excited by the Raman transition and detected in an interface-selective manner. From a parallel point of view, vibrational sum-frequency spectroscopy provides an interface-selective IR spectroscopy, in which the vibrational coherence is created in the IR resonant transition. In addition to these two methods, electronic sum-frequency spectroscopy has recently been invented.[51, 52] This provides UV-VIS absorption spectrum with interface selectivity as an elegant extension of wavelength-dependent second-harmonic generation spectroscopy.

Physical chemistry in condensed phases has been developed by using bulk-sensitive UV-VIS, IR, and Raman spectroscopy. We now have a good start to make *chemistry at buried interfaces* by combining the interface-selective analogues of the three representative methods for chemical analysis.

Acknowledgments

The principle and experimental results of fourth-order coherent Raman spectroscopy reviewed in sections 2-6 were developed in collaboration with Satoru Fujiyoshi and Taka-aki Ishibashi. The spectrum of a solution-TiO_2 interface presented in section 7 is an original result obtained by the authors. Fruitful discussion with Kazuya Watanabe and Shoichi Yamaguchi is acknowledged. These studies have been performed with the support of Kanagawa Academy of Science and Technology, Core Research for Evolutional Science and Technology of the Japan Science and Technology Agency, and from a Grant-in-Aid for Scientific Research in Priority Area “Molecular Nano Dynamics” from the Ministry of Education, Culture, Sports, Science and Technology.

Notes and references

1. X. D. Zhu, H. Suhr and Y. R. Shen, *Phys. Rev. B,*, 1987, 35, 3047.
2. G. A. Somorjai and G. Rupprechter, *J. Phys. Chem.*, 1999, 103, 1623.
3. A. Bandara, S. S. Kano, K. Onda, S. Katano, J. Kubota, K. Domen, C. Hirose and A. Wada, *Bull. Chem. Soc. Jpn.*, 2002, 75, 1125.
4. R. D. Schaller, J. C. Johnson, K. R. Wilson, L. F. Lee, L. H. Haber and R. J. Saykally, *J. Phys. Chem. B*, 2002, 106, 5143.
5. T. Ishibashi and H. Onishi, *Chemistry Letters*, 2004, 33, 1404-1407.
6. M. M. Knock, G. R. Bell, E. K. Hill, H. J. Turner and C. D. Bain, *J. Phys. Chem. B*, 2003, 107, 10801.
7. S. Ye, S. Nihonyanagi and K. Uosaki, *Phys. Chem. Chem. Phys.*, 2001, 3, 3463.
8. L. F. Scatena, M. G. Brown and G. L. Richmond, *Science*, 2001, 292, 908.
9. J. Wang, M. Even, X. Chen, A. H. Schmaier, J. H. Waite and Z. Chen, *J. Am. Chem. Soc.* , 2003, 125, 9914.
10. Y. M. Chang, L. Xu and H. W. K. Tom, *Phys. Rev. Lett.*, 1997, 78, 4649.
11. A. A. Mani, Z. D. Shultz, Y. Caudano, B. Champagne, C. Humbert, L. Dreesen, A. A. Gewirth, J. O. White, P. A. Thiry and A. Peremans, *J. Phys. Chem. B*, 2004, 108, 16135.
12. R. Braun, B. D. Casson, C. D. Bain, E. W. M. van der Ham, Q. H. F. Vrehen, E. R. Eliel, A. M. Brigg and P. B. Davies, *J. Chem. Phys.*, 1999, 110, 4634.
13. Y. Matsumoto and K. Watanabe, *Chem. Rev.*, 2006, 106, 4234.
14. L. Dhar, J. A. Rogers and K. A. Nelson, *Chem. Rev.*, 1994, 94, 157.
15. T. Dekorsy, G. C. Cho and H. Kurz, in *Light Scatteringin Solids VIII*, eds. M. Cardona and G. Güntherodt, Springer, Editon edn., 2000, p. chapter 4.
16. T. E. Stevens, J. Kuhl and R. Merlin, *Phys. Rev. B*, 2002, 65, 144304.
17. S. Fujiyoshi, T. Ishibashi and H. Onishi, *J. Phys. Chem. B*, 2004, 108, 1525-1528.
18. S. Fujiyoshi, T. Ishibashi and H. Onishi, *Journal of Molecular Structure*, 2005, 735-736, 169-177.
19. D. A. Long, *Raman Spectroscopy*, McGraw-Hill, New York, 1977.
20. L. D. Ziegler, R. Fan, A. E. Desrosiers and N. F. Sherer, *J. Chem. Phys.*, 1994, 100, 1823.
21. S. R. Meech and K. Yoshihara, *J. Phys. Chem.*, 1990, 94, 4913.
22. A. Castro, V. Sitzmann, D. Zhang and K. B. Eisenthal, *J. Phys. Chem.*, 1991, 95, 6752.
23. X. Shi, B. Borguet, A. N. Tarnovsky and K. B. Eisental, *Chem. Phys.*, 1996, 205, 167.
24. R. Antoine, A. A. Tamburello-Luca, P. Hebért, P. F. Brevet and H. H. Girault, *Chem. Phys. Lett.*, 1998, 288, 138.
25. D. Zimdars, J. I. Dadap, K. B. Eisenthal and T. F. Heinz, *Chem. Phys, Lett.*, 1999, 301, 112.
26. D. A. Steinhurst and J. C. Owrutsky, *J. Phys. Chem. B*, 2001, 105, 3062.
27. K. Kemnitz, K. Bhattacharyya, J. M. Hicks, G. R. Pinto, B. Eisenthal and T. F. Heinz, *Chem. Phys, Lett.*, 1986, 131, 285.
28. G. Berkovic, Y. R. Shen, G. Marowsky and R. Steinhoff, *J. Opt. Soc. Am. B*, 1989, 6, 205.
29. W. Ostroverkhov, G. A. Waychunas and Y. R. Shen, *Phys. Rev. Lett.*, 2005, 94, 046102.
30. Y. Hirose, H. Yui and T. Sawada, *J. Phys. Chem. B*, 2005, 109, 13063.
31. S. Fujiyoshi, T. Ishibashi and H. Onishi, *J. Phys. Chem. B*, 2006, 110, 9571.
32. S. Fujiyoshi, T. Ishibashi and H. Onishi, *J. Phys. Chem. B*, 2004, 108, 10636.
33. K. Watanabe, N. Takagi and Y. Matsumoto, *Chem. Phys. Lett.*, 2002, 366, 606.
34. K. Watanabe, N. Takagi and Y. Matsumoto, *Phys. Rev. Lett.*, 2004, 92, 057401.
35. K. Watanabe, N. Takagi and Y. Matsumoto, *Phys. Rev. B*, 2005, 71, 085414.
36. M. Fuyukui, K. Watanabe and Y. Matsumoto, *Phys. Rev. B*, 2006, 74, 195412.
37. K. Watanabe, N. Takagi and Y. Matsumoto, *Phys. Chem. Chem. Phys.*, 2005, 7, 2697.
38. A. V. Melnikov, I. Radu, U. Bovensiepen, O. Krupin, K. Starke, E. Matthias and M. Wolf, *Phys. Rev. Lett.*, 2003, 91, 227403.
39. A. V. Melnikov, I. Radu, U. Bovensiepen, K. Starke, M. Wolf and E. Matthias, *J. Opt. Soc. Am. B*, 2005, 22, 204.
40. U. Diebold, *Surf. Sci. Rept.*, 2003, 48, 53.
41. H. Onishi, K. Fukui and Y. Iwasawa, *Bull. Chem. Soc. Jpn.*, 1995, 68, 2447.
42. J. M. White, J. Szanyi and M. A. Henderson, *J. Phys. Chem. B*, 2003, 107, 9029.
43. S. Fujiyoshi, T. Ishibashi and H. Onishi, *J. Phys. Chem. B*, 2005, 109, 8557-8561.
44. D. M. Eagels, *J. Phys. Chem. Solids*, 1964, 25, 1243.
45. S. P. S. Proto, P. A. Fleury and T. C. Damen, *Phys. Rev.*, 1967, 154, 522.
46. G. Rocker, J. A. Schaefer and W. Göpel, *Phys. Rev. B*, 1984, 30, 3704.
47. P. A. Cox, R. G. Egdell, S. Eriksen and W. R. Flavell, *Journal of Electron Spectroscopy and Related Phenomena*, 1986, 39, 117.
48. Y.-M. Chang, *Appl. Phys. Lett.*, 2003, 82, 1781.
49. Y.-M. Chang, H. H. Lin, C. T. Chia and Y. F. Chen, *Appl. Phys. Lett.*, 2004, 84, 2548.
50. S. Yamaguchi and T. Tahara, *J. Phys. Chem. B*, 2005, 109, 24211.
51. S. Yamaguchi and T. Tahara, *J. Phys. Chem. B*, 2004, 108, 19079.
52. S. Yamaguchi and T. Tahara, *J. Chem. Phys.*, 2006, 125, 194711.

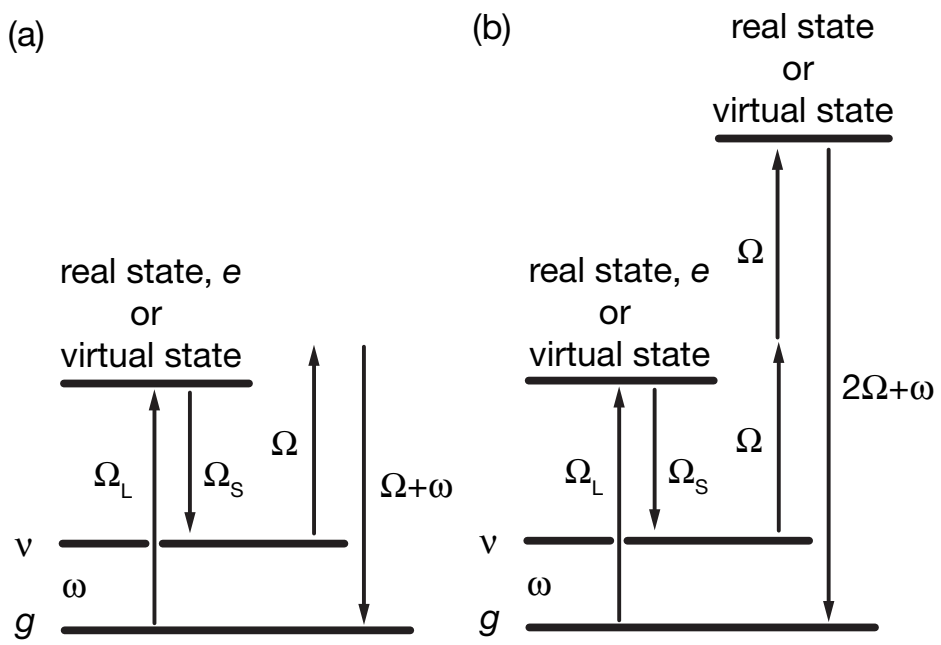
(a)
real state, e
or
virtual state
Ω_L
Ω_S
Ω
Ω+ω
ν
ω
g
(b)
real state
or
virtual state
Ω
real state, e
or
virtual state
2Ω+ω
Ω
Ω_L
Ω_S
ν
ω
g

Fig. 1

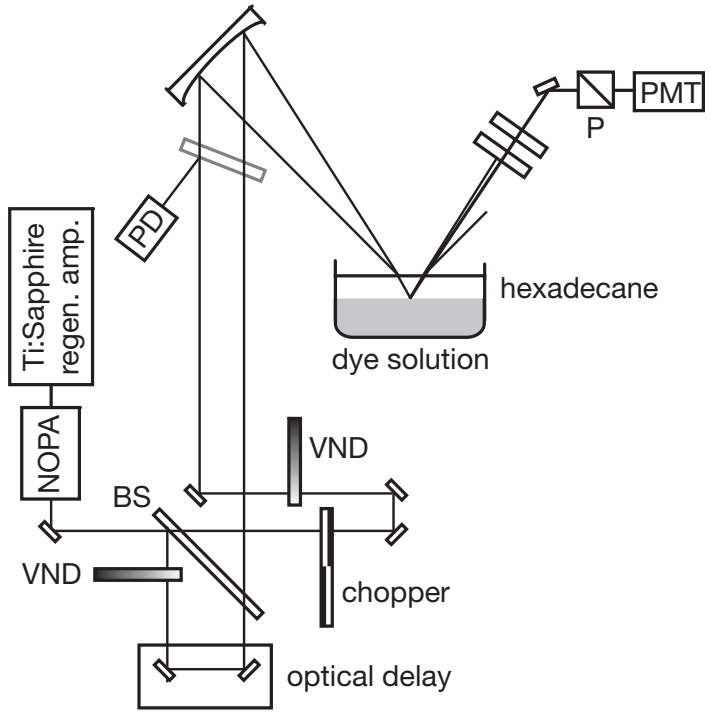
PMT
P
PD
Ti:Sapphire
regen. amp.
hexadecane
dye solution
NOPA
VND
BS
VND
chopper
optical delay

Fig. 2

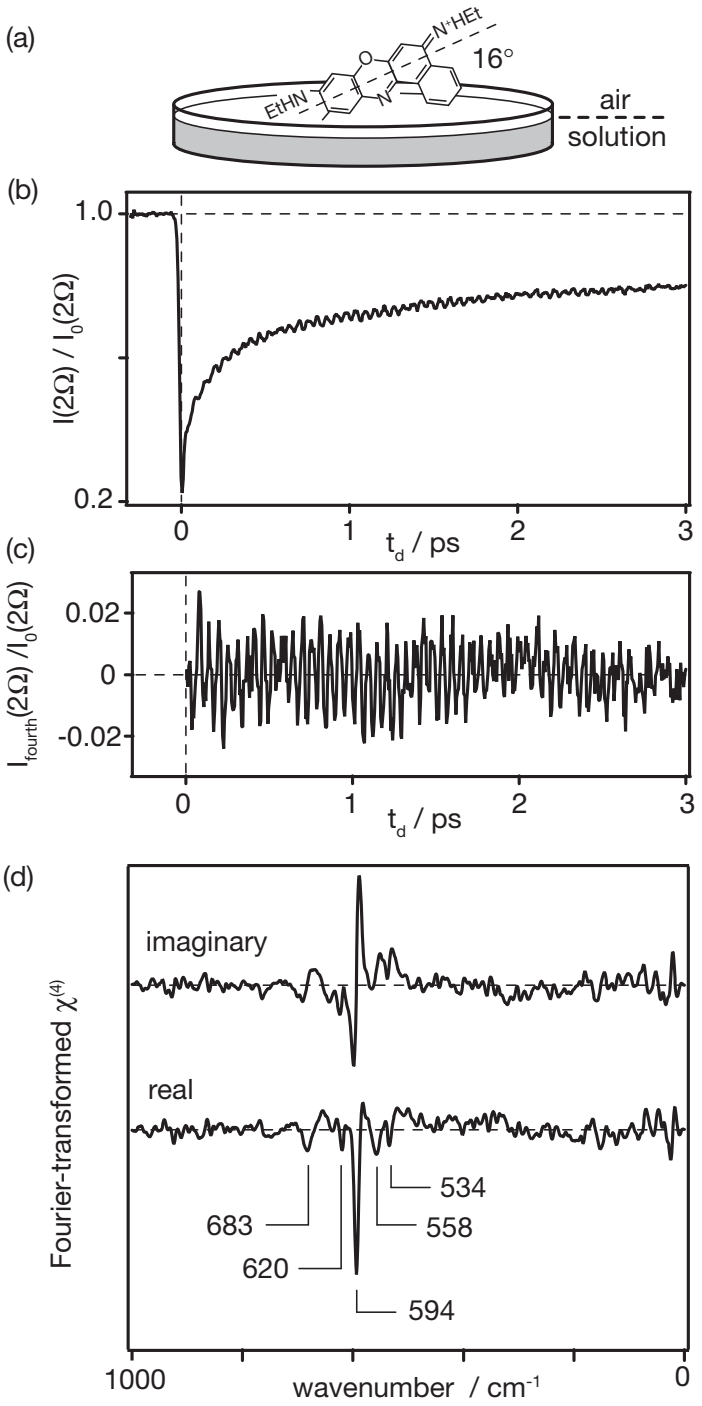
(a)
N+HEt
16°
EtHN
O
N
air
solution
(b)
1.0
0.2
I(2Ω) / I0(2Ω)
0
1
2
3
td / ps
(c)
0.02
0
-0.02
Ifourth(2Ω) /I0(2Ω)
0
1
2
3
td / ps
(d)
imaginary
real
Fourier-transformed χ(4)
683
620
534
558
594
1000
wavenumber / cm-1
0

Fig. 3

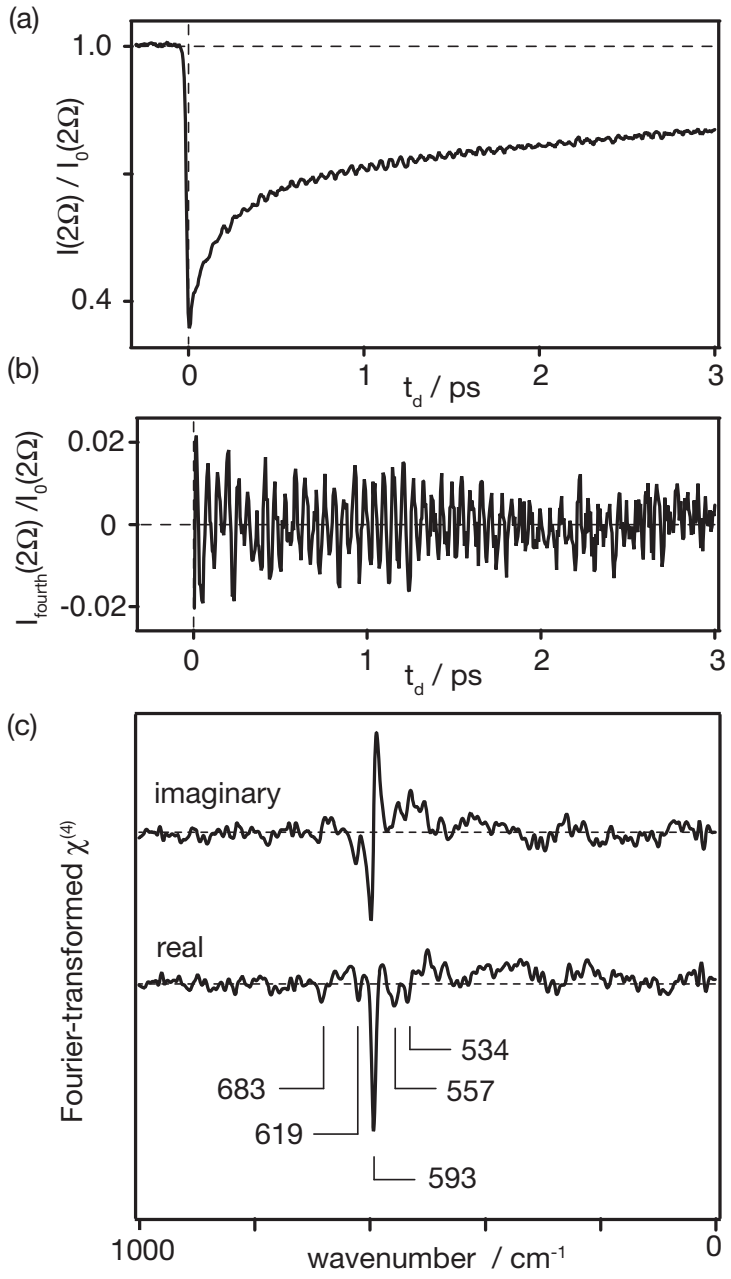
(a)
1.0
0.4
I(2Ω) / I0(2Ω)
0
1
2
3
td / ps
(b)
0.02
0
-0.02
Ifourth(2Ω) /I0(2Ω)
0
1
2
3
td / ps
(c)
imaginary
real
Fourier-transformed χ(4)
534
557
683
619
593
1000
wavenumber / cm-1
0

Fig. 4

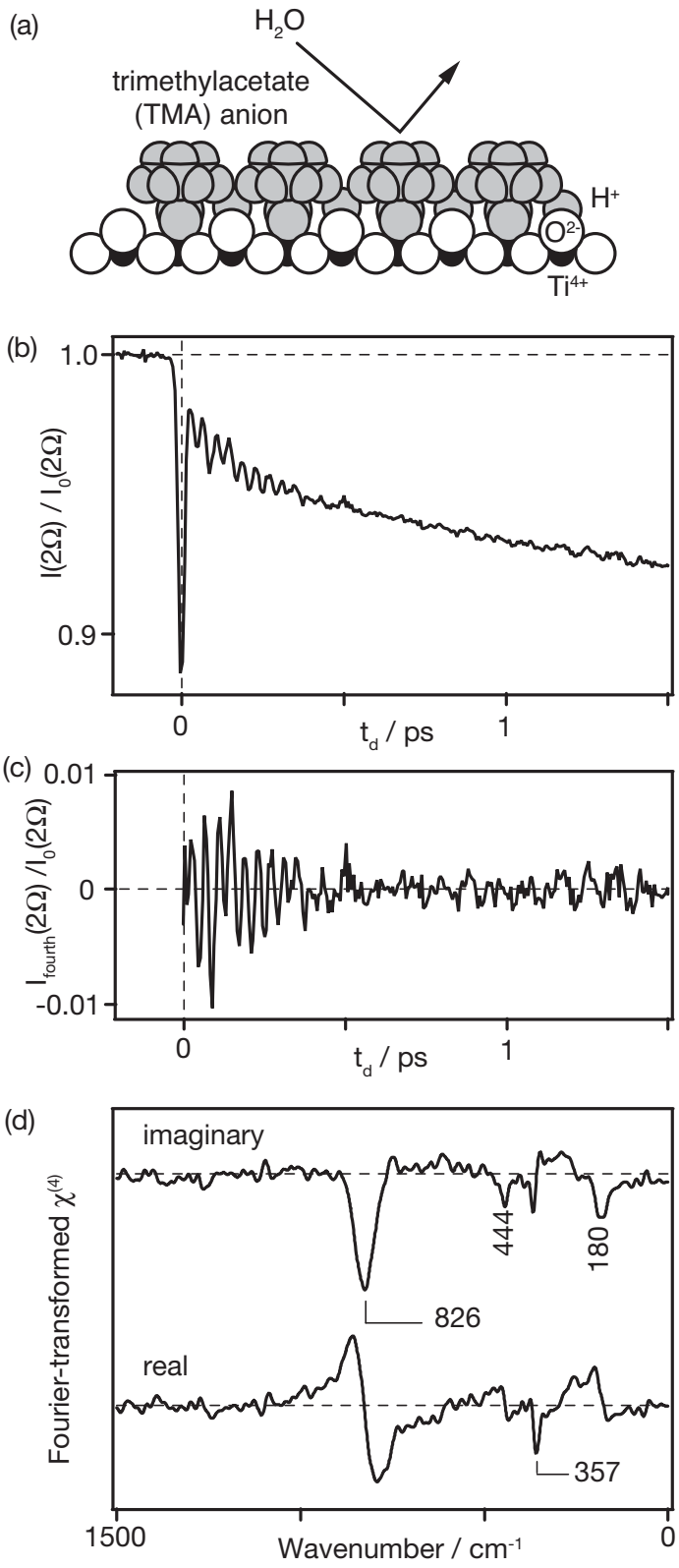
(a)
H2O
trimethylacetate
(TMA) anion
H+
O2-
Ti4+
(b)
1.0
0.9
I(2Ω) / I0(2Ω)
0
td / ps
1
(c)
0.01
0
-0.01
Ifourth(2Ω) /I0(2Ω)
0
td / ps
1
(d)
imaginary
444
180
826
real
357
Fourier-transformed χ(4)
1500
Wavenumber / cm-1
0

Fig. 5

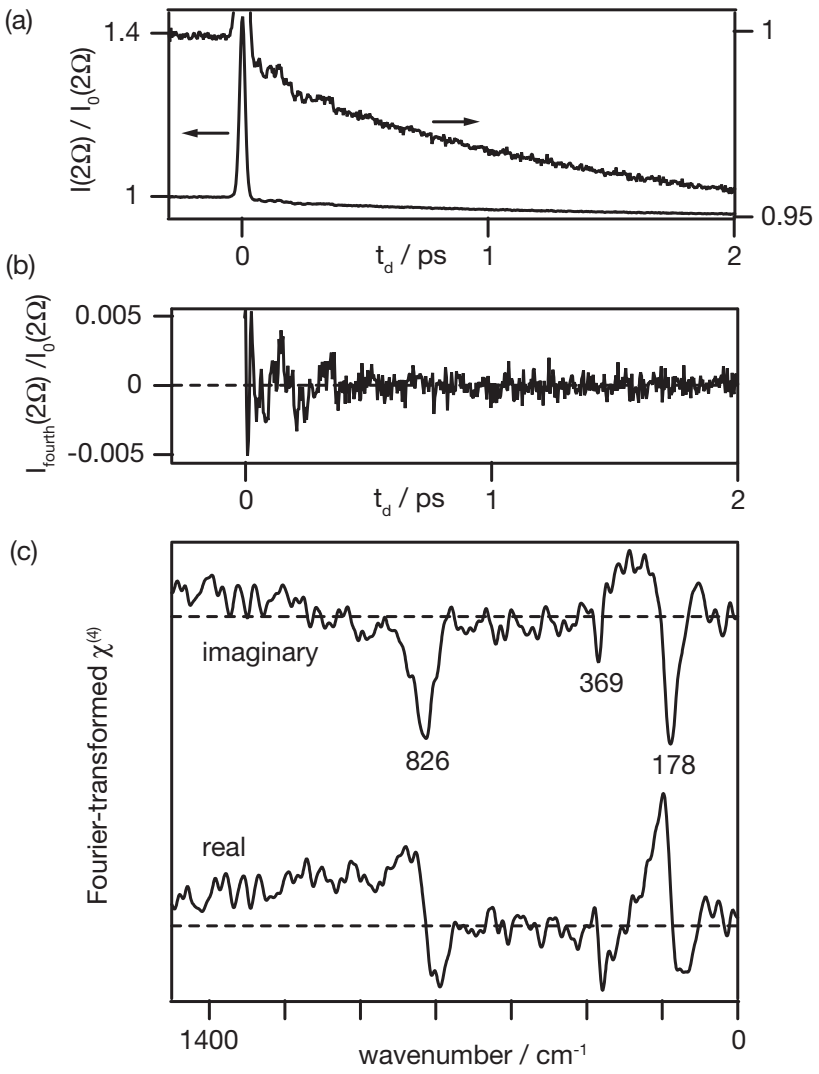
(a)
1.4
1
I(2Ω) / I0(2Ω)
1
0.95
0
td / ps
1
2
(b)
0.005
0
-0.005
Ifourth(2Ω) /I0(2Ω)
0
td / ps
1
2
(c)
imaginary
369
826
178
real
Fourier-transformed χ(4)
1400
0
wavenumber / cm-1

Fig. 6